J. Phys.: Condens. Matter **9** (1997) 7105–7118. Printed in the UK PII: S0953-8984(97)83865-9

An *ab initio* Hartree–Fock study of the magnetic states of the polymorphs of MnS

R I Hines†, N L Allan†, G S Bell‡ and W C Mackrodt‡

† School of Chemistry, University of Bristol, Cantocks Close, Bristol BS8 1TS, UK

‡ School of Chemistry, University of St Andrews, St Andrews, Fife KY16 9ST, UK

Received 29 April 1997, in final form 23 June 1997

Abstract. Periodic unrestricted Hartree–Fock calculations are shown to predict the correct low-temperature magnetic phases of α-MnS (AF_2) and both cubic and hexagonal forms of β-MnS (AF_3). The high-spin insulating nature of MnS is also correctly predicted with local moments close to those derived from neutron scattering factors. MnS in all its forms is shown to be a largely ionic p→d charge transfer system with a predominantly $d^5\underline{L}$ first ionized state.

1. Introduction

It has been a widely held view that the transition metal chalcoginides are strongly correlated systems [1] with the implication that single-particle theories in general, and Hartree–Fock theory in particular, are unlikely to give a qualitatively correct description of their ground state electronic structures. However, recent studies of MnO and NiO [2], Li-doped NiO [3], α-Fe_2O_3 [4], α-Cr_2O_3 [5], $MnFe_2O_4$ [6] and $KCuF_3$ [7] have shown that spin polarized (unrestricted) Hartree–Fock theory (UHF) is able to account for their wide-band-gap insulating behaviour and predict the correct low-temperature magnetic states, including spin–lattice interactions in MnO and NiO [2] and $KCuF_3$ [7].

In this paper we extend these studies [2–6] to a wider range of systems and turn attention to the three different polymorphs of MnS for which there are reliable magnetic data. They are α-MnS, which possesses the NaCl structure like MnO, and β-MnS in both the (cubic) zinc-blende and (hexagonal) wurtzite structures. In the first two, Mn ions form face-centred cubic arrays and in the third a hexagonal close-packed array, so that in each case every Mn has twelve nearest Mn neighbours. In α-MnS, where S ions occupy the octahedral interstices of the cation array, nearest Mn neighbours are bridged by S in a *perpendicular* Mn–S–Mn configuration, while the six next-nearest Mn neighbours are connected via *linear* Mn–S–Mn linkages. By way of contrast, in both forms of β-MnS S ions occupy tetrahedral interstices in the cation sub-lattice so that each Mn is linked tetrahedrally through S to its twelve nearest Mn neighbours. The three structures and Mn arrangements are illustrated in figure 1. Thus with their range of structures and diversity of possible magnetic orderings, the α- and β-polymorphs of MnS provide a further severe test of Hartree–Fock methodology.

The occurrence of these different crystalline forms of MnS raises important questions as to the nature of the magnetic states in each. All three appear to be antiferromagnetic [8] with Néel temperatures in the range 75–150 K. This compares with a value [2] of 116 K for MnO, which suggests comparable magnetic coupling in the two systems. α-MnS possesses the same AF_2 antiferromagnetic structure as MnO, in which the individual atomic

0953-8984/97/347105+14$19.50

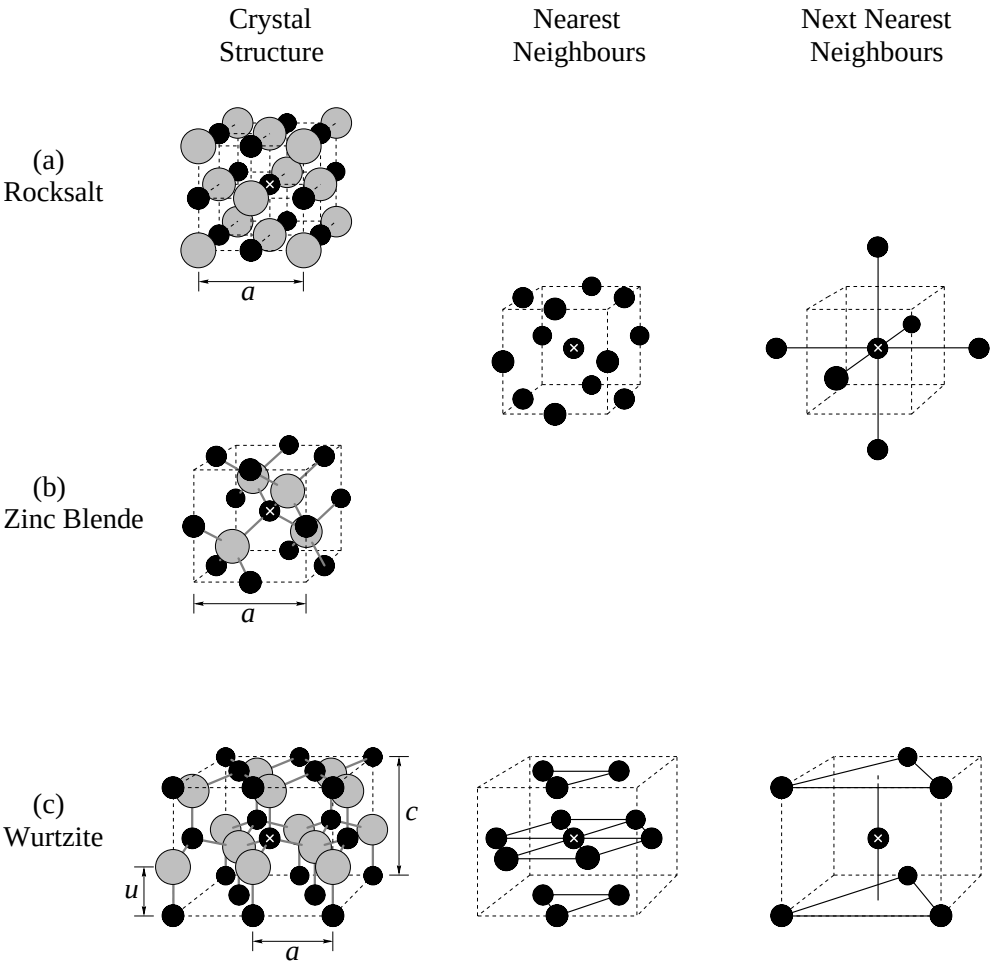

Figure 1. Crystal structures, nearest-cation-neighbour arrangment, and next-nearest-cation arrangement in the rocksalt (α-MnS), zinc-blende (cubic β-MnS) and wurtzite (hexagonal β-MnS) forms of MnS. Lattice parameters and, where appropriate, internal degrees of freedom, are also marked.

moments are aligned in {111} ferromagnetic sheets, with adjacent sheets having antiparallel spins (figure 2). The AF_1 spin arrangement (figure 2), in which the spin alignment of adjacent {100} ferromagnetic sheets is antiparallel, does not appear to have been observed. The zinc-blende form of β-MnS where the Mn atoms have the same spatial arrangement as in the rocksalt structure, shows neither of these magnetic arrangements, but instead an AF_3-type ordering shown in figure 2. Here the alignment of spins in {210} ferromagnetic sheets is parallel to that of one of its two neighbouring planes, and antiparallel to the other. Following Anderson's pioneering work in this area, antiferromagnetism in cubic systems of this sort is most often discussed in terms of the relative number of ferromagnetic and antiferromagnetic interactions involving nearest and next-nearest magnetic neighbours respectively (figure 1 and table 1). In AF_1 ordering two-thirds of nearest-neighbour pairs are aligned antiferromagnetically, while the remaining nearest neighbours and all the next-nearest neighbours are aligned ferromagnetically. In the AF_2 arrangement, there are equal

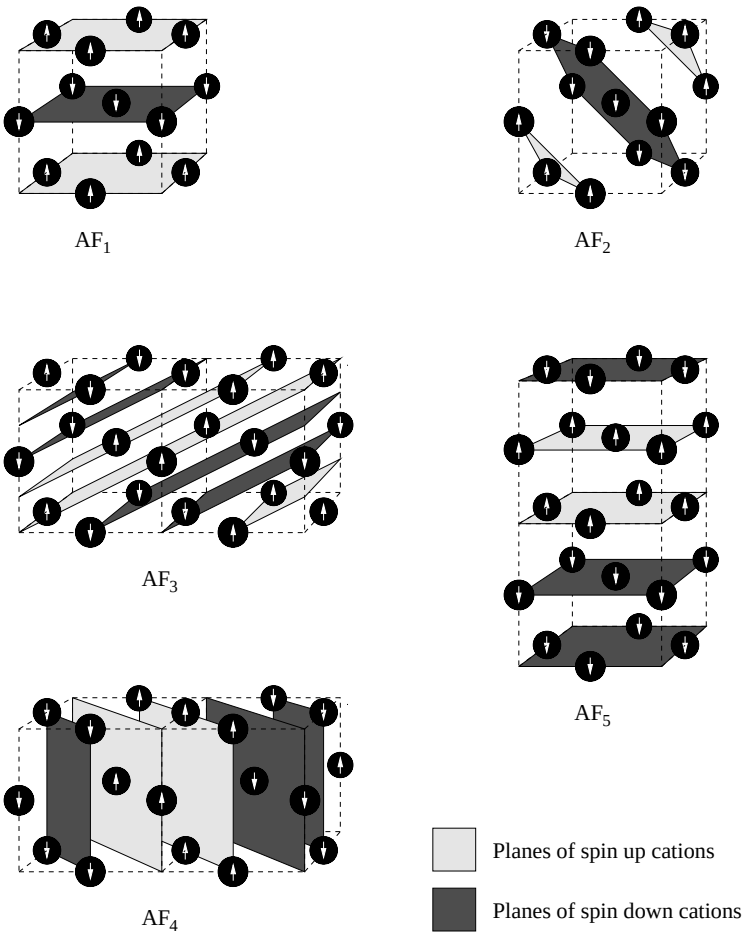

Figure 2. AF_1, AF_2, AF_3, AF_4 and AF_5 magnetic orderings for a fcc lattice.

numbers of ferromagnetically and antiferromagetically aligned nearest neighbours while all next-nearest neighbours are antiferromagnetically aligned. The same nearest-neighbour alignment is present in AF_3 ordering as in AF_1; but, of the next-nearest neighbours, one-third are antiparallel and two-thirds parallel, as opposed to an all-parallel arrangement in AF_1. Figure 1 and table 1 also show the orderings in two further possible structures—AF_4 and AF_5.

Table 1. Number of parallel and antiparallel nearest neighbours (nn) and next-nearest neighbours (nnn) for each type of antiferromagnetic ordering.

		AF_1	AF_2	AF_3	AF_4	AF_5
nn	$\uparrow\downarrow$	8	6	8	6	4
	$\uparrow\uparrow$	4	6	4	6	8
nnn	$\uparrow\downarrow$	0	6	2	4	2
	$\uparrow\uparrow$	6	0	4	2	4

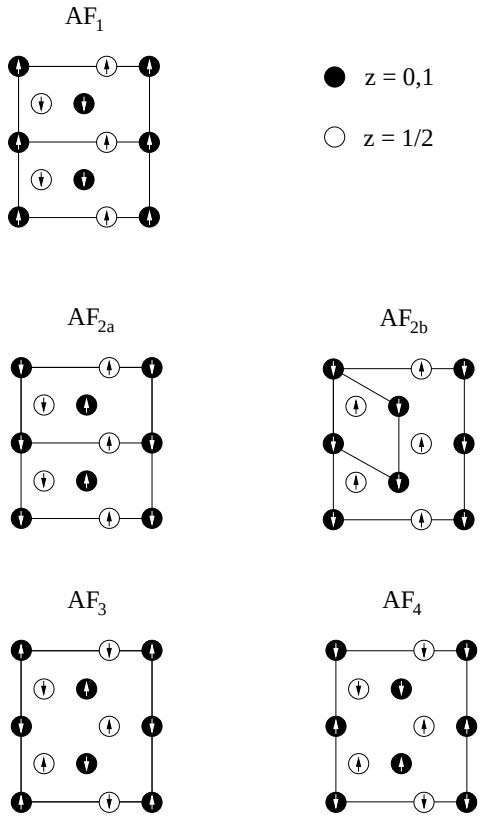

Figure 3. Possible magnetic orderings in hexagonal β-MnS consistent with the observed unit cell size.

The observed magnetic ordering (AF_3) in the hexagonal wurtzite form of β-MnS, shown in figure 3, is more complicated than in the cubic polymorphs, for neutron diffraction studies indicate that the magnetic unit cell is four times that determined from x-ray crystallography. There are other possible arrangements subject to the restrictions that the magnetic unit cell is no larger than that observed and that each cation has the same distribution of parallel and antiparallel nearest and next-nearest cation neighbours. These are also shown in figure 3 and are labelled according to the nearest- and next-nearest-neighbour alignments, analogously to the ccp case (table 1). The observed magnetic order is analogous to the AF_3 arrangement observed in the ccp cation array. Both forms of β-MnS comprise linked SMn_4 tetrahedra and, as shown in figure 4, the spin arrangement in each close-packed Mn plane is the same in both, although the individual stacking depends on whether the array is cubic or hexagonal close packed.

A commonly favoured qualitative explanation for these differences in magnetic structure invokes superexchange [9], which is particularly favoured in the NaCl-type structures where there are *linear* next-nearest-neighbour Mn–S–Mn linkages. In both forms of β-MnS the bond angle in the nearest-neighbour Mn–S–Mn linkages is tetrahedral. If superexchange is also operative here, some antiferromagnetic alignment between nearest neighbours might be expected. This is indeed the case for the AF_1 and AF_3 arrangements which contain the largest number of nearest-neighbour antiferromagnetic interactions.

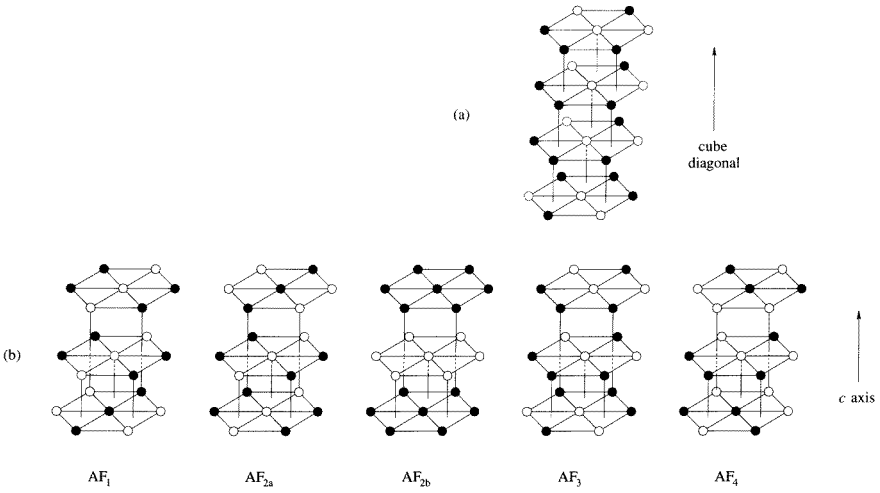

Figure 4. Stacking of close-packed cation planes for (a) cubic β-MnS (AF_3 only) and (b) hexagonal β-MnS (AF_1–AF_4) arrangements. For comparison, in the cubic AF_2 structure, adopted by α-MnS, the spins in adjacent close-packed (111) planes are antiparallel (figure 2). Filled and empty circles denote cations of opposite spin.

2. Theoretical methods

The calculations reported here were carried out using the all-electron *ab initio* LCAO periodic Hartree–Fock method as described in detail previously [10] and implemented in the CRYSTAL95 computer code [11]. As before [2–6], an essential feature of the calculations is the use of the UHF procedure of Pople and Nesbet [12] to describe the high-spin d^5 configuration of Mn and different crystalline spin arrangements. The practical solution of the Hartree–Fock equations for periodic systems introduces numerical approximations which originate in the integration over reciprocal space to reconstruct the electronic distribution and in the evaluation of the Coulomb and exchange series. In these series the Gaussian integrals are classified according to overlap or penetration criteria. Integrals of sufficiently low overlap are neglected or approximated, the cutoffs being controlled by five parameters, discussed in detail elsewhere [13]. In this paper calculations were performed with tolerances set to 10^{-7}, 10^{-7}, 10^{-7}, 10^{-7} and 10^{-14}, which provide high numerical accuracy, as in several recent studies [14]. The reciprocal space integration was performed by sampling the Brillouin zone at a regular set of points defined by a shrinking factor of 8 and 3 for the cubic and wurtzite structures respectively and the criterion for self-consistency taken as a change in the total unit-cell energy of 10^{-5} mHa for consecutive SCF cycles.

The localized crystal orbitals consisted of 25 atomic orbitals for Mn and 21 for S of the type

Mn: 1s(8)2sp(6)3sp(4)4sp(1)5sp(1)3d(4)4d(1)

S: 1s(8)2sp(6)3sp(4)4sp(1)5sp(1)3d(1)

where the numbers in brackets are the numbers of Gaussian functions used to describe the corresponding shell, e.g. 1s, 2sp, 3d etc. The core basis set for Mn—1s(8)2sp(6)3sp(4)—was the same as that used previously [2] for MnO and the initial sulphur basis set that reported for MgS in [15], with a fourth function added to the 3sp shell. The exponents

and contraction coefficients for the 4sp, 5sp, 3d and 4d shells of Mn and 3sp, 4sp, 5sp and 3d shells on S were then re-optimized by minimizing the ground-state energy of the fcc rock-salt structure for a primitive ferromagnetic unit cell at the experimental lattice parameter. The final basis sets for both Mn and S are listed in table 2. Calculations for the various magnetic states reported here were performed on supercells obtained by appropriate expansion of the primitive unit-cell vectors.

Table 2. Core and valence basis sets for MnS.

		Mn			S		
No	Shell type	Exponent	Coefficients		Exponent	Coefficients	
	Core bases						
1	s	292 601.0	0.000 227		109 211.0	0.000 252 0	
		42 265.0	0.001 9		16 235.206	0.001 993 4	
		8 947.29	0.011 1		3 573.028 6	0.011 117 7	
		2330.32	0.050 1		943.238 11	0.049 894 5	
		702.047	0.170 5		287.261 79	0.166 145 5	
		242.907	0.369 1		99.914 226	0.362 701 8	
		94.955	0.403 5		38.602 137	0.410 878 7	
		39.577 7	0.143 7		15.531 224	0.145 787 5	
2	sp	732.14	−0.005 3	0.008 6	281.221 71	−0.005 778 0	0.008 142 7
		175.551	−0.067 3	0.061 2	67.106 575	−0.066 585 5	0.056 557 0
		58.509 3	−0.129 3	0.213 5	21.794 135	−0.120 355 2	0.203 958 2
		23.129	0.253 5	0.401 8	8.209 764 6	0.274 131 0	0.397 332 8
		9.753 6	0.634 5	0.401 2	3.417 828 9	0.646 382 9	0.394 631 3
		3.454 5	0.271 4	0.222 2	1.545 222 5	0.292 579 2	0.154 434 5
3	sp	38.389	0.015 7	−0.031 1	4.279 0	−0.190 0	−0.061 1
		15.436 7	−0.253 5	−0.096 9	1.752 8	−0.604 0	0.133 0
		6.178 1	−0.864 8	0.256 3	0.688 4	0.824 6	1.142 8
		2.823 5	0.933 7	1.655 2	0.216 5	0.786 4	0.501 4
	Valence bases						
4	sp	1.192 2	1.0	1.0	0.289 9	1.0	1.0
5	sp	0.481 9	1.0	1.0	0.105 9	1.0	1.0
6	d	22.933 7	0.070 0		0.345 2	1.0	
		6.260 5	0.303 8		—	—	
		2.105 2	0.547 2		—	—	
		0.761 0	0.516 0		—	—	
7	d	0.267 2	1.0		—	—	

The main source of error in the Hartree–Fock method is the neglect of electron correlation which originates directly from the use of a single determinant to represent the many-body wavefunction. As a result, binding energies tend to be underestimated by about 30% and lattice constants generally by ≈2%. These can be improved by introducing *a posteriori* correlation corrections based on a range of correlation functionals and the Hartree–Fock electron densities [16].

3. Results

Previous UHF calculations for MnO and NiO found energy-minimized (optimized) lattice structures to be very nearly independent of the magnetic state [2]. Accordingly, we based our structural optimizations of the three polymorphs reported here on the primitive ferromagnetic

(FM) unit cell which in every case we found to be high-spin insulating. The calculated UHF lattice parameters are listed in table 3 together with the corresponding experimental values. These lattice parameters are around 5% greater than the experimental values for the antiferromagnetic materials, which is consistent with earlier work [2] on MnO and NiO, even though the percentage error is somewhat larger. The *a posteriori* inclusion of correlation corrections to the Hartree–Fock energy based on the correlation-only functional of either Perdew [17] or Becke [18] reduces this discrepancy, which in the case of the Perdew functional, is less than 0.5% for the rocksalt and zinc-blende structures and less than 3% for the wurtzite structure as shown in table 3.

Table 3. Calculated and experimental structures for MnS.

Structure	Lattice parameter	Experiment	HF	HF + corr. [17]
Rocksalt	a (Å)	5.224 [22]	5.4232	5.2407
Zinc blende	a (Å)	5.600 [23]	5.9030	5.6138
	a (Å)	3.976	4.2039	4.0832
Wurtzite	c (Å)	6.432 [23]	6.7388	6.5851
	u	—	0.3812	0.3812

Table 4 shows that the energies of the Hartree–Fock optimized rock-salt, zinc-blende and wurtzite structures of MnS for all six spin arrangements are in the order

$$E_{HF}(\text{wurtzite}) < E_{HF}(\text{zinc blende}) < E_{HF}(\text{rock salt})$$

which is contrary to experiment, whereas the corresponding order at the *experimental* geometries is

$$E_{HF}(\text{rock salt}) < E_{HF}(\text{wurtzite}) < E_{HF}(\text{zinc blende}).$$

The inclusion of *a posteriori* correlation corrections, based again on the correlation-only functionals due to either Perdew [17] or to Becke [18] reduces the optimized lattice parameters and the rock-salt structure is lower in energy at both the experimental and Hartree–Fock geometries. Total energies based on the Perdew functional are tabulated in table 4.

The order of the Hartree–Fock energies of the different magnetic states is also given in table 4. This lists the energy differences between the FM and the possible antiferromagnetic states at (i) the experimental geometry and (ii) the optimized Hartree–Fock geometry for the FM arrangement. The cost of the calculations precluded an exhaustive study of these energies as a function of geometry. However, for the rocksalt structure where such a study was feasible, the difference between the optimized AF_2 and FM lattice parameters at the Hartree–Fock level was found to be negligible, which confirmed that the extra cost of such calculations is not justified.

For α-MnS the Hartree–Fock energy ordering for both geometries, i.e. (i) and (ii), is

$$AF_2 < AF_4 < AF_3 < AF_5 < AF_1 < FM$$

and so the predicted low-temperature spin arrangement, AF_2, agrees with that observed. Furthermore, the inclusion of correlation energy corrections does not change this order.

We turn now to β-MnS in the zinc-blende structure, for which table 4 contains the corresponding energies to those for the rocksalt structure. The Hartree–Fock energy ordering, at both geometries, is

$$AF_3 < AF_1 < AF_2 < AF_4 < AF_5 < FM.$$

Table 4. Energies (au) per formula unit of the different structures and magnetic orderings for MnS. Results are for (i) the experimental structure (ii) the optimized geometry predicted for the ferromagnetic ordering at the Hartree–Fock level. Both Hartree–Fock energies and energies incorporating *a posteriori* correlation correction [17] are listed. The energies for each set of antiferromagnetic arrangments are relative to that of the corresponding ferromagnetic state.

Crystal structure	Magnetic structure	(i) Experimental geometry		(ii) Optimized HF geometry	
		E_{HF} (au)	E_{HF} + corr (au)	E_{HF} (au)	E_{HF} + corr (au)
	Ferromagnetic	−1547.485 493	−1549.362 220	−1547.493 028	−1549.358 996
Rocksalt	AF_1	-0.058×10^{-3}	-0.149×10^{-3}	-0.005×10^{-3}	-0.048×10^{-3}
	AF_2	-0.429×10^{-3}	-0.887×10^{-3}	-0.187×10^{-3}	-0.518×10^{-3}
	AF_3	-0.209×10^{-3}	-0.440×10^{-3}	-0.080×10^{-3}	-0.253×10^{-3}
	AF_4	-0.326×10^{-3}	-0.666×10^{-3}	-0.140×10^{-3}	-0.380×10^{-3}
	AF_5	-0.188×10^{-3}	-0.377×10^{-3}	-0.079×10^{-3}	-0.209×10^{-3}
	Ferromagnetic	−1547.482 917	−1549.349 553	−1547.493 367	−1549.345 373
Zinc-blende	AF_1	-1.291×10^{-3}	-2.353×10^{-3}	-0.596×10^{-3}	-0.827×10^{-3}
	AF_2	-0.981×10^{-3}	-1.731×10^{-3}	-0.452×10^{-3}	-0.624×10^{-3}
	AF_3	-1.304×10^{-3}	-2.399×10^{-3}	-0.600×10^{-3}	-0.838×10^{-3}
	AF_4	-0.980×10^{-3}	-1.750×10^{-3}	-0.450×10^{-3}	-0.630×10^{-3}
	AF_5	-0.648×10^{-3}	-1.165×10^{-3}	-0.296×10^{-3}	-0.418×10^{-3}
	Ferromagnetic	−1547.483 386	−1549.348 272	−1547.494 373	−1549.346 387
	AF_1	-1.986×10^{-3}	-2.227×10^{-3}	-1.030×10^{-3}	-1.099×10^{-3}
Wurtzite	AF_{2a}	-1.715×10^{-3}	-1.862×10^{-3}	-0.897×10^{-3}	-0.915×10^{-3}
	AF_{2b}	-0.815×10^{-3}	-1.073×10^{-3}	-0.397×10^{-3}	-0.542×10^{-3}
	AF_3	-2.390×10^{-3}	-2.631×10^{-3}	—	—
	AF_4	-2.116×10^{-3}	-2.262×10^{-3}	—	—

For both geometries, therefore, the AF_3 state is predicted to be lowest in energy, as found experimentally, which is a particularly encouraging result for periodic UHF calculations. The differences between the AF_3 and AF_1 energies, and between the AF_2 and AF_4 energies are small—the nearest-neighbour coupling is the same for the two sets of spin arrangements.

For β-MnS in the wurtzite structure the calculated energy ordering at the experimental geometry is

$$AF_3 < AF_4 < AF_1 < AF_{2a} < AF_{2b} < FM$$

where the lowest-energy structure is, again, that observed. Here the expense of the calculations for the largest unit cells (AF_3, AF_4) precluded the investigation of any other geometries. An inspection of the crystal structures suggests that there is a correlation between the relative energies and the number of (unfavourable) collinear FM Mn–Mn–Mn linkages in the close-packed planes. For example, the possible stacking sequences for β-MnS (figure 4) show that all the close-packed planes in the AF_{2b} structure, which is predicted to be the highest-energy antiferromagnetic phase, have only collinear FM Mn–Mn–Mn arrangements. The difference in energy between the AF_{2b} and AF_{2a} structures gives an estimate of this effect and can be used to rationalize the relative energy of AF_4. Similar considerations apply to the relative ordering of the spin arrangements within the wurtzite phase compared to the zinc-blende phase, e.g., the relative position of the AF_4 structure in the two series.

The calculated magnetic moment of α-MnS is 4.92 μ_B (4.89 μ_B at the experimental geometry) which compares with an experimental value [19] of 4.54 μ_B. Correlation effects would tend to decrease the predicted moment while spin–orbit coupling, which is not

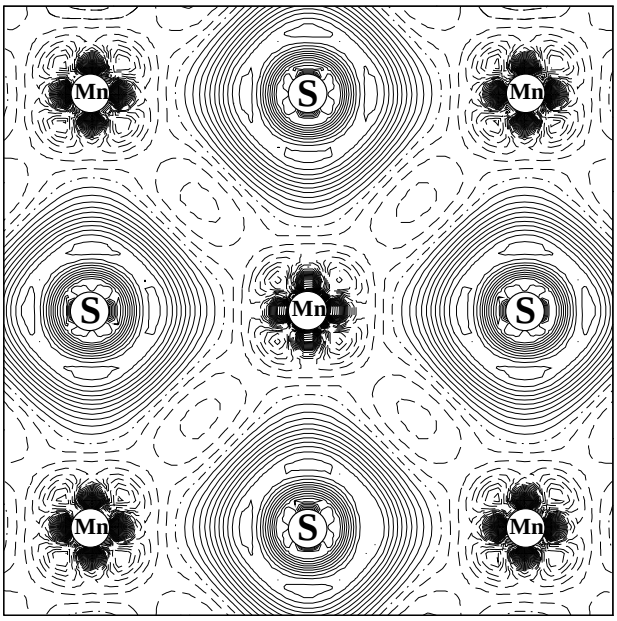

(*a*)

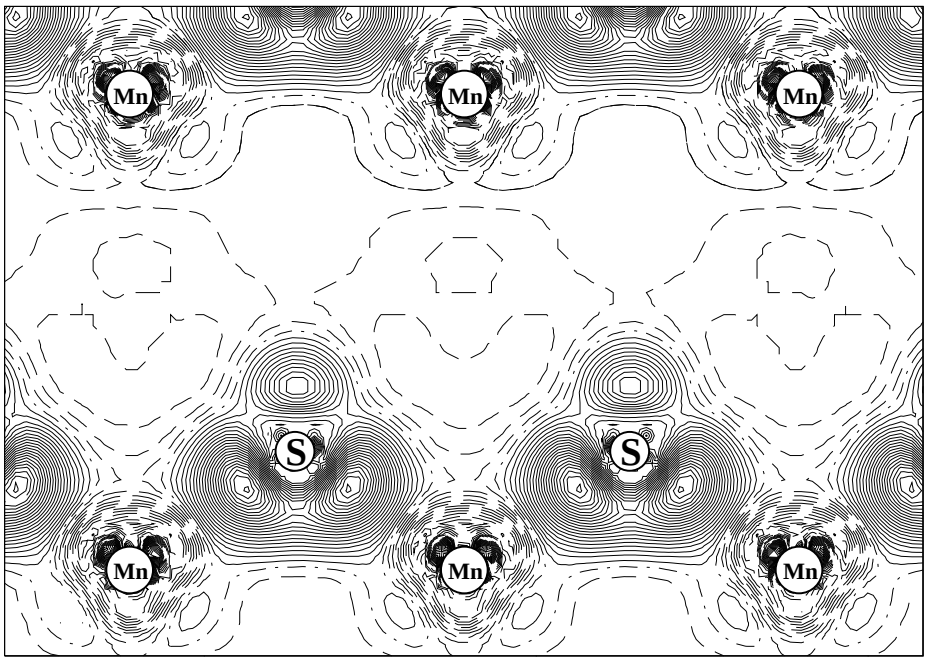

(*b*)

Figure 5. Electron density difference maps (bulk minus free ion superposition): (a) basal (001) plane of the AF_2 structure of α-MnS; (b) (011) plane of cubic β-MnS structure (AF_3); (c) $(1\bar{2}10)$ plane of hexagonal β-MnS (AF_3). All these maps were calculated using the experimental geometry. Continuous, dashed and dot–dashed lines correspond to positive, negative and zero values respectively. The separation between adjacent isodensity curves is 0.001 e bohr^{-3}.

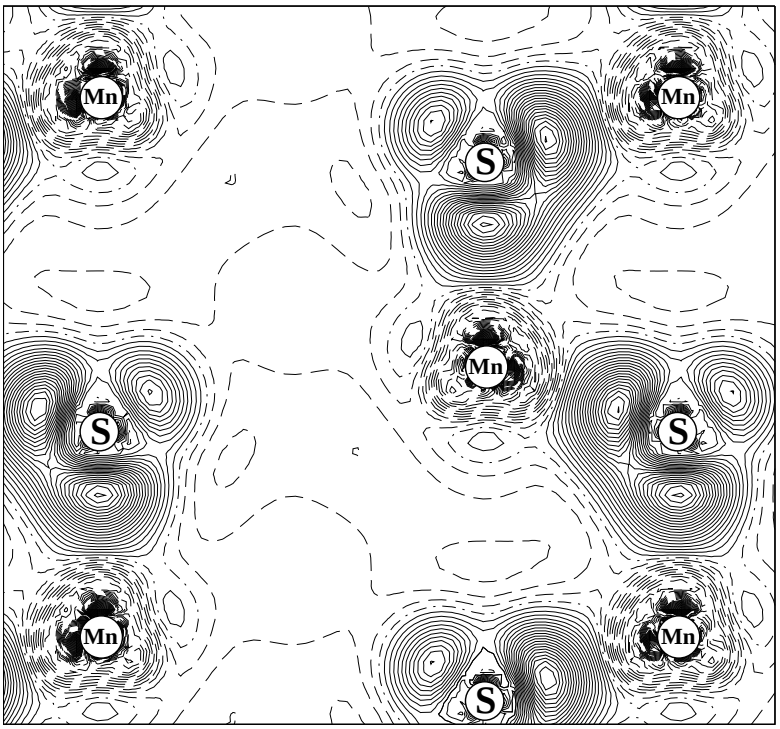

Figure 5. Continued.

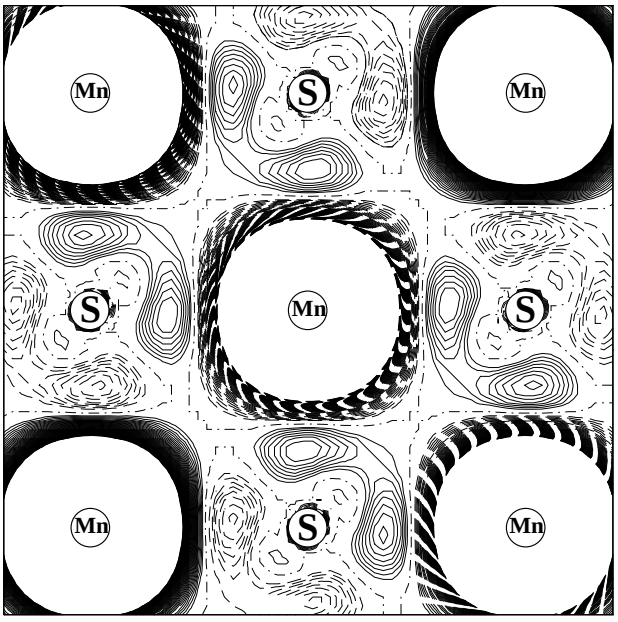

Figure 6. Spin density map in the basal (001) plane of the AF_2 structure of α-MnS. Continuous, dashed and dot–dashed lines correspond to positive, negative and zero values respectively. The separation between adjacent isodensity curves is 0.0002 e bohr^{-3}.

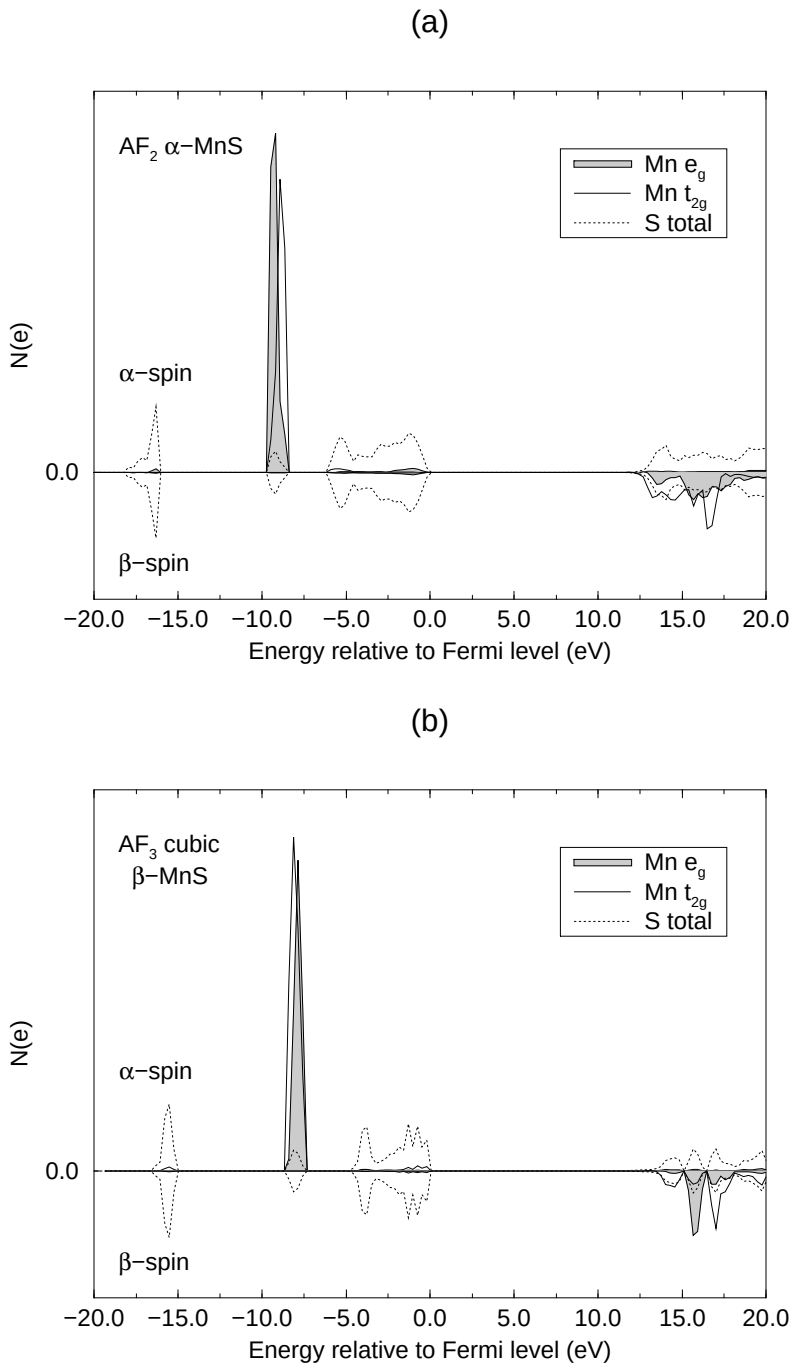

Figure 7. Band-projected density of states for (a) α-MnS (AF_2) (b) cubic β-MnS (AF_3) (c) hexagonal β-MnS (AF_3). All these were calculated at the experimental geometry.

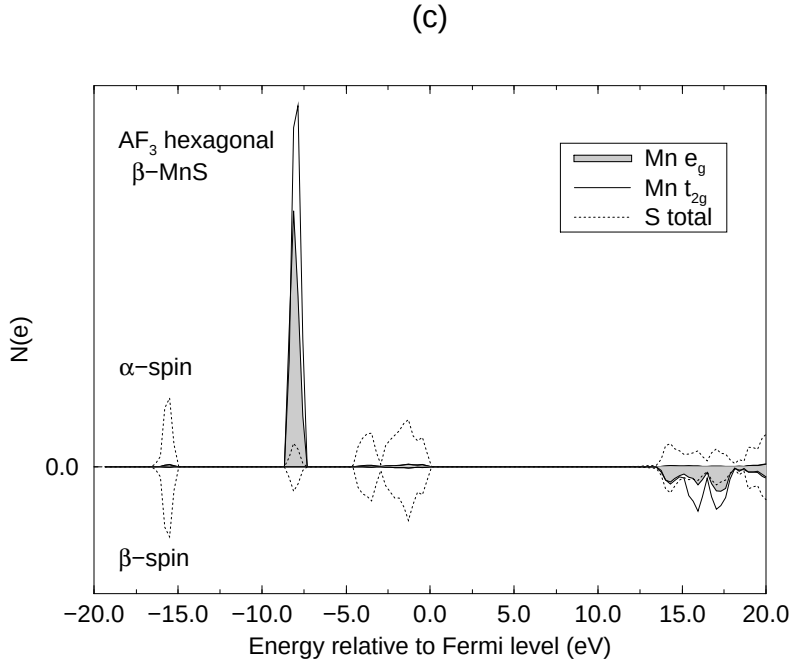

Figure 7. Continued.

included in the calculations reported here, would tend to increase it. Since the experimental value is not measured directly, a more useful comparison would be between the experimental and theoretical neutron-scattering factors.

In α-MnS the observed ground-state spin arrangement of successively antiparallel ferromagnetic (111) planes gives rise to a magnetostriction (spin–lattice interaction) in which there is a rhombohedral contraction normal to the ferromagnetic planes. At low temperature the crystal axes are inclined at $\approx 0.09^\circ$ from the ideal cubic directions [20]. We have calculated the variation of the total energy of both the FM and AF_2 configurations as a function of a volume-conserving rhombohedral distortion based on the experimental lattice constant. As expected no distortion from cubic symmetry was found for the FM spin arrangement, whereas the calculated equilibrium deviation from the ideal cubic angle for the AF_2 arrangement is 0.05°.

Table 5. Mulliken charges $q(e)$, 3d populations n_{3d}, and net atomic spins δn_S(Mn) and δn_S(S) for the three forms of MnS considered in this study.

	Experimental geometry				Optimized HF geometry			
Structure	q	n_{3d}	δn_S(Mn)	δn_S(S)	q	n_{3d}	δn_S(Mn)	δn_S(S)
α-MnS (AF_2)	1.828	5.126	4.892	0.000	1.854	5.101	4.919	0.000
Cubic β-MnS (AF_3)	1.799	5.123	4.875	0.000	1.830	5.100	4.915	0.000
Hexagonal β-MnS (AF_3)	1.803	5.121	4.877	0.003	—	—	—	—

Turning now to the electronic structure of MnS, Mulliken population analyses indicate atomic charges of around $\pm 1.8\ e$ for all the structures which suggests substantial ionicity.

This is supported by the 3d and net spin populations given in table 5, which are roughly the same, and the magnitude and sign of the MnS overlap population. Further insight into the electronic structure is contained in the charge and spin density distributions, which are obtained *directly* from the wavefunction, and also from difference density distributions, which are obtained by subtracting the *atomic* charge distributions (derived from the free ion wave functions) from those of the bulk crystal. Figure 5(a), which shows the difference density distribution in a basal (001) plane of the AF_2 structure of α-MnS, indicates that there is a significant contraction of the atomic orbitals of both the anion and cation relative to the free ion due to the Madelung field and Pauli repulsion, as in the case of MnO [2]. Figure 5(b) shows a similar difference density in a (011) plane of cubic β-MnS for the AF_3 structure, in which the strong polarization of the S valence orbitals can be clearly seen. This is also evident in the $(1\bar{2}10)$ plane of hexagonal β-MnS (figure 5(c)). There is also very small spin polarization on S evident in the spin density difference ($N_\alpha - N_\beta$) for the AF_2 structure (figure 6), showing a shift of the α-electron density towards the Mn ion with β polarization and vice versa.

Atom-projected valence band densities of states (DOS) provide further evidence of the ionicity of MnS. Figure 7 shows these for the AF_2 structure of α-MnS and the AF_3 structures of cubic and hexagonal β-MnS, where α and β spin denote majority and minority spins respectively. As is well known the band gap [21] is overestimated in Hartree–Fock theory. Unlike MnO [2] the majority weight of the Mn(d) states lies well below the upper valence bands which consist of essentially unpolarized S(p) states with negligible Mn(d) density in this region. Thus UHF calculations predict MnS to be a charge transfer insulator and its first ionized state predominantly $d^5\underline{L}$. Finally we note that like MnO the insulating characteristics of MnS derive from the large on-site Coulomb energy which separates the filled and unfilled d states.

4. Conclusions

The principal conclusions of this study are (i) that UHF calculations predict the correct low-temperature magnetic phases of α-MnS (AF_2) and both forms of β-MnS (AF_3); (ii) that they also predict correctly the high-spin insulating nature of MnS with local moments which are close to those derived from neutron scattering factors; (iii) that MnS in all its forms is predicted to be a largely ionic p→d charge transfer system with a predominantly $d^5\underline{L}$ first ionized state.

Acknowledgments

This work was supported by EPSRC grants GR/K06389 and GR/L31340. RIH thanks the EPSRC for financial support.

References

[1] Hüfner S 1994 *Adv. Phys.* **43** 183
[2] Towler M D, Allan N L, Harrison N M, Saunders V R, Mackrodt W C and Aprà E 1994 *Phys. Rev.* B **50** 5041
[3] Mackrodt W C, Harrison N M, Saunders V R, Allan N L and Towler M D 1996 *Chem. Phys. Lett.* **250** 66
[4] Catti M, Valerio G and Dovesi R 1995 *Phys. Rev.* B **51** 7441
[5] Catti M, Sandrone G, Valerio G and Dovesi R 1996 *J. Phys. Chem. Solids* **57** 1735
[6] Mackrodt W C and Simson E-A 1996 *J. Chem. Soc. Faraday Trans.* **92** 2043

[7] Towler M D, Dovesi R and Saunders V R 1995 *Phys. Rev.* B **52** 10 150
[8] Corliss L, Elliott N and Hastings J 1956 *Phys. Rev.* **104** 924
[9] Anderson P W 1959 *Phys. Rev.* **115** 2
[10] Pisani C, Dovesi R and Roetti C 1989 *Hartree-Fock Ab Initio Treatment of Crystalline Systems* (Berlin: Springer)
[11] Dovesi R, Saunders V R and Roetti C 1995 *Crystal 95, User Manual* (Università di Torino and CCL Daresbury Laboratory)
[12] Pople J A and Nesbet R K 1954 *J. Chem. Phys.* **22** 571
[13] Dovesi R, Causà M, Orlando R, Roetti C and Saunders V R 1990 *J. Chem. Phys.* **92** 7402
[14] See, for example, Dovesi R, Ricart J M, Saunders V R and Orlando R 1995 *J. Phys.: Condens. Matter* **7** 7997
Ricart J M, Dovesi R, Roetti C and Saunders V R 1995 *Phys. Rev.* B **52** 2381
[15] Lichanot A, Dargelos A, Larrieu C and Orlando R 1994 *Solid State Commun.* **90** 189
[16] See, for example, Causà M and Zupan A 1994 *Chem. Phys. Lett.* **220** 145
Causà M and Zupan A 1995 *Int. J. Quant. Chem.* **28** 633
[17] Perdew J P 1991 *Electronic Structure of Solids '91* ed P Ziesche and H Eschrig (Berlin: Akademie)
Perdew J P, Chevary J A, Vosko S H, Jackson K A, Pederson M R, Singh D J and Fiolhais C 1992 *Phys. Rev.* B **46** 6671
[18] Becke A D 1988 *J. Chem. Phys.* **88** 2547
[19] Fender B E F, Jacobson A J and Wedgwood F A 1968 *J. Chem. Phys.* **48** 990
[20] van der Heide H, van Bruggen C F, Wiegers G A and Haas C 1983 *J. Phys. C: Solid State Phys.* **16** 855
[21] Goede O, Heimbrodt W, Lamla M and Weinhold V 1988 *Phys. Status Solidi* b **146** K65
Sato H, Mihara T, Furuta A, Ueda Y, Namatame H and Taniguchi M 1996 *J. Electron Spectrosc. Relat. Phenom.* **78** 87
[22] Bayliss P, Erd D C, Mrose M E, Sabina A P and Smith D K (eds) 1986 *Mineral Powder Diffraction File: Data Book* (Swarthmore, PA: International Centre for Diffraction Data)
[23] Wyckoff R W G 1963 *Crystal Structures* 2nd edn (New York: Interscience)